Article:

Arndt, T., Laity, P.R., Johansson, J. et al. (2 more authors) (2021) Native-like flow properties of an artificial spider silk dope. ACS Biomaterials Science & Engineering, 7 (2). pp. 462-471. ISSN 2373-9878

https://doi.org/10.1021/acsbiomaterials.0c01308

ACS Biomaterials SCIENCE & ENGINEERING

ACS AUTHORCHOICE

pubs.acs.org/journal/abseba

Article

Native-like Flow Properties of an Artificial Spider Silk Dope

Tina Arndt, Peter R. Laity, Jan Johansson, Chris Holland,* and Anna Rising*

Cite This: ACS Biomater. Sci. Eng. 2021, 7, 462−471

Read Online

ACCESS | Metrics & More | Article Recommendations | Supporting Information

ABSTRACT: Recombinant spider silk has emerged as a biomaterial that can circumvent problems associated with synthetic and naturally derived polymers, while still fulfilling the potential of the native material. The artificial spider silk protein NT2RepCT can be produced and spun into fibers without the use of harsh chemicals and here we evaluate key properties of NT2RepCT dope at native-like concentrations. We show that NT2RepCT recapitulates not only the overall secondary structure content of a native silk dope but also emulates its viscoelastic rheological properties. We propose that these properties are key to biomimetic spinning and that optimization of rheological properties could facilitate successful spinning of artificial dopes into fibers.

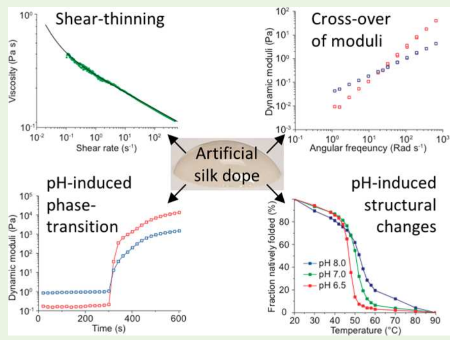

KEYWORDS: *recombinant spider silk proteins, biomimetic materials, rheology, protein secondary structure*

INTRODUCTION

The extreme toughness of spider silk, combined with properties like biological degradability and biocompatibility, make it a highly attractive material for a wide variety of technical and medical applications.[1,2] In order to make this material reproducible, available, and economical, industrial-scale production of spider-silk mimics are best produced recombinantly, where silk proteins (spidroins) are expressed in heterologous hosts, purified, and subsequently spun into fibers. However, we are faced with a challenge; the vast majority of available protocols for spidroin production include the use of denaturing agents during purification and/or coagulation baths during spinning.[3] These conditions may be incompatible with the native protein conformation and will likely result in fibers with a molecular structure that differs from that of the native fiber.[4]

Native spider silk fibers are spun from specialized silk glands localized in the opisthosoma. There are seven types of glands, of which the major ampullate gland and the fiber it produces, the dragline silk, are most extensively studied.[4−7] Prior to spinning the spidroins contained within major ampullate glands are stored at very high concentrations and near neutral pH (30−50% w/v, > 6.3 pH) as a soluble, transparent and viscous substance (dope).[6,8] As the dope passes through the gland into the spinning duct the microenvironment is significantly altered, i.e., the pH decreases to at least 5.7, the salt concentration changes and shear stress and pulling forces act on the proteins.[8−12] Together, these factors induce fiber formation where the proteins' secondary structures transition from being predominantly α-helices and random coils to the ordered β-sheet-rich structures observed in the fiber.[12−18]

The rheological properties of the dope are fundamental for native silk spinning.[19,20] Key features of the native dope include high viscosity, crossover of the viscous and elastic moduli, and perhaps most importantly, shear-thinning behavior.[21] Along the silk duct, the inner diameter decreases significantly; consequently, the flow results in increased extensional and shear stresses acting on the dope.[11,22] Shear-thinning appears to be a prerequisite for spinning, as it allows the viscous dope to transit more easily through the duct and reduces the energy requirements for spinning.[11,23−25] Thus, it is attractive to generate artificial spinning dopes with rheological properties resembling those of native silk feedstock, particularly as the properties of the dope likely influence the properties of spun fibers.[26,27] Yet, so far recombinant spidroin dopes have failed to recapitulate all of the key properties of the native dope.[27,28]

Recently, we described the first biomimetic spinning procedure, which opens up the possibility to produce biomaterials from artificial spider silk without involving harsh chemicals.[29] We have developed a chimeric minispidroin (NT2RepCT) that is as soluble as native spidroins (can be concentrated to 50% w/v), gives high production yields, and requires only aqueous buffers for purification, concentration, and spinning. The assembly of NT2RepCT is pH dependent

Received: September 3, 2020
Accepted: December 22, 2020
Published: January 4, 2021

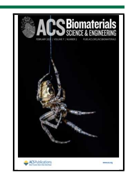

https://dx.doi.org/10.1021/acsbiomaterials.0c01308
ACS Biomater. Sci. Eng. 2021, 7, 462−471

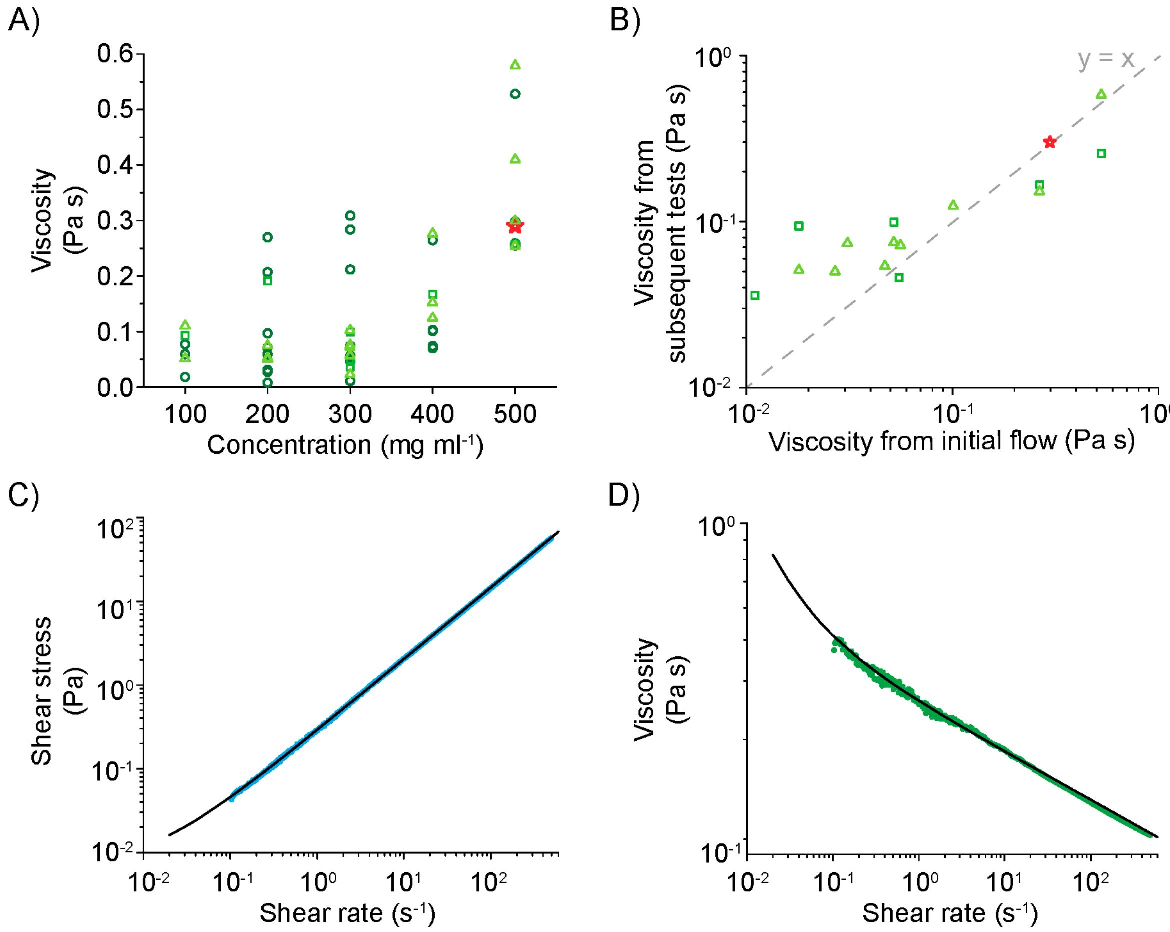

Figure 1. Rheological characterization of recombinant NT2RepCT dope. (A) Viscosity at 25 °C and a shear rate of 1 s^{-1} for different NT2RepCT concentrations, measured over the final 30 s during a 100 s steady shear flow (circles represent fresh specimens, squares represent specimens remeasured following previous, nondestructive tests) or during shear rate ramps (average from 0.9 to 1.1 s^{-1}, triangles), (shear stress and viscosity data for a representative specimen indicated by red star are shown in C and D). (B) Correlation between shear viscosities at 1 s^{-1}, from initial measurements and subsequent steady flow (squares) or shear rate ramps (triangles). As a guide to the eye, the dashed line represents $y = x$. (C, D) Shear stress and viscosity of a 500 mg mL^{-1} NT2RepCT specimen during a shear rate ramp from 0.1 to 500 s^{-1}; the solid lines represent the best fits using the Herschel−Bulkley model (eqs 1a−c).

and recapitulates important molecular mechanisms associated with native silk spinning.[29,30]

Having already demonstrated that it may be spun under conditions similar to those of natural silk fibers, we explore the properties of NT2RepCT spinning dope using rheology, circular dichroism (CD) spectroscopy and Fourier transform infrared (FTIR) spectroscopy. In particular, we observe similarities in flow behavior and protein conformations, between aqueous solutions of this recombinant protein and those published for native dopes.

EXPERIMENTAL SECTION

Expression and Purification of NT2RepCT. Protein expression and purification was performed essentially as previously described.[29] Briefly, the NT2RepCT construct is composed of a His6-tag, a N-terminal domain (NT) from *Euprosthenops australis* MaSp1, a repetitive part consisting of two poly alanine and two glycine-rich repeat regions from *E. australis* MaSp1 and a C-terminal domain (CT) from *Araneus ventricosus* minor ampullate spidroin. Transformed BL21 (DE3) *E. coli* cells were grown in LB broth, Miller, (VWR) at 37 °C supplemented with kanamycin (BioChemica PanReac AppliChem ITW Reag) until OD_{600} reached 0.9. The expression was induced by adding IPTG (VWR) and the cells were further incubated at 20 °C overnight. The culture was harvested and lysed in a high-pressure cell disrupter (T-S Series Machine, Constant Systems Limited) and the soluble fraction was purified by Ni-IMAC gravitational flow chromatography. The protein solution was dialyzed against 20 mM Tris-HCl, pH 8 (VWR) and SDS-PAGE (BioRad) was used for quality control. The NT2RepCT protein solution was concentrated to 100−500 mg mL^{-1} using centrifugal concentrators (Vivaspin 20, 10 kDa MWCO, GE Healthcare), which is similar to the concentration of native dope (300−500 mg mL^{-1}).[6] The protein concentration was determined spectrophotometrically (Biophotometer, Eppendorf) and the protein was kept at -20°C until further use.

Rheological Analysis of NT2RepCT Dope. The flow characteristics of NT2RepCT solutions of different concentrations were measured using a Discovery HR2 rheometer (TA Instruments) fitted with a "1/20" stainless steel cone (20 mm diameter; 1° opening angle) and a Peltier temperature-controlled lower plate. To prevent water evaporation from the specimen, several water droplets were placed onto the lower plate, (around but not touching the specimen) and a loose-fitting cover was used to maintain saturated humidity around the specimen (as has proved effective in other works). After loading and allowing the specimen (70 μL) to come to temperature (25 °C), it was subjected to a steady shear flow over 100 s at a shear rate ($\dot{\gamma}$) of 1 s^{-1}, in order to establish consistent conditions (i.e., superseding previous flow history); the shear stress and viscosity (σ and η) were evaluated by averaging the data from the final 30 s. Oscillatory data was recorded at 25 °C from 20 to 0.1 Hz, using 2 or 5% strain amplitude. (Both values were within the linear viscoelastic

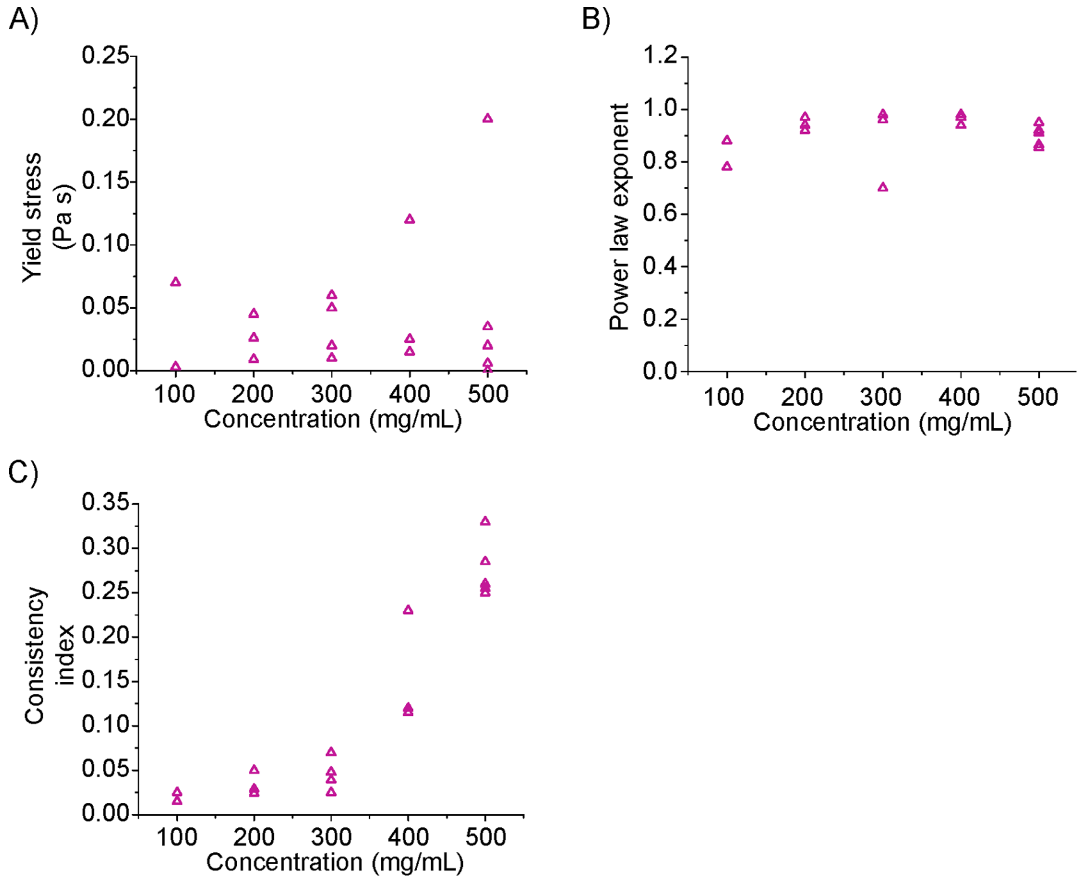

Figure 2. Rheological parameters obtained by fitting the Herschel-Bulkley model (eqs 1a−c) to data from shear rate ramp measurements for NT2RepCT solutions at 25 °C: (A) yield stress, (B) power law coefficient, (C) consistency index.

strain region, and the higher amplitude provided better sensitivity at lower frequencies.) Shear rate dependence of flow behavior was measured using a logarithmic ramp from $\dot{\gamma}$ = 0.1 to 500 s^{-1} over 10 min. For comparison, an aqueous solution of poly(*N*-isopropyl-acrylamide) of appropriate concentration and molecular weight (pNiPAm, 40 kDa, 330 mg mL^{-1}) was measured at constant at 1 s^{-1} constant shear rate over 100 s at 25 °C.

In order to observe the effect of acidification, a few drops of glacial acetic acid were pipetted onto tissue paper, which was placed into the humidity chamber during the oscillatory measurements.

Circular Dichroism (CD) Spectroscopy of NT2RepCT. The buffer of NT2RepCT was exchanged by gel filtration on a PD-10 column (GE Healthcare) for 20 mM sodium phosphate (pH 8.0, 7.0, 6.5, and 6.0, respectively, Merck). Experiments were performed in a J-1500 CD spectrometer (JASCO, USA) using 300 μL cuvettes with 1 mm path length. For all measurements, the protein was diluted to 5 μM in 20 mM sodium phosphate buffer. Temperature scans were performed between 21 to 90 °C at a heating rate of 1 °C min^{-1} and spectra were recorded from 260 to 175 nm. Afterward, the samples were cooled to 20 °C for 15 min and spectra were recorded to investigate the reversibility of the conformational changes. For each temperature, five scans were performed to calculate the means and were then smoothed. Thermal unfolding curves were plotted by using the molar residual ellipticity at 222 nm. The fraction natively folded was converted from the ellipticity at 222 nm with the formula $(CD_{measured} - CD_{end})/(CD_{start} - CD_{end})$.

Fourier Transform Infrared (FTIR) Spectroscopy of NT2RepCT. Infrared (IR) spectra were collected at 37 °C in reflectance geometry, from 800 to 4000 cm^{-1}, using a Fourier-transform spectrometer (Nicolet 380, Thermo-Electron Corp. Madison, WI, USA) fitted with a deuterated triglycine sulfate (DTGS) detector and thermostatic "Golden gate" attenuated total reflectance (ATR, SpecAc, UK) sample stage with a diamond element. The optical path through the spectrometer and ATR device were purged with dry, filtered air to minimize interference due to atmospheric CO_2 and water vapor. Liquid specimens were placed directly onto the ATR element, covered with a glass coverslip, and sealed around the edges with petroleum jelly to prevent evaporation, and 64 scans were collected at 4 cm^{-1} resolution.

RESULTS

NT2RepCT Shows Non-Newtonian Behavior and Viscoelastic Properties. We chose to initially study the viscosity and shear-thinning behavior of NT2RepCT because these are two main characteristics of native dope.[23,24] The viscosities of recombinant NT2RepCT dopes were tested at 100, 200, 300, 400, and 500 mg mL^{-1}, wherein the three higher concentrations match the concentration of spidroins in silk glands.[6] The results are presented in Figure 1.

The shear viscosities were low (all below 1 Pa s) in view of the concentrations investigated (up to 500 mg mL^{-1}). To put this in context, an aqueous solution of pNiPAm of similar molecular weight and concentration (40 kDa, 330 g L^{-1}) exhibited a shear viscosity of 4.0 Pa s (7 specimens, range 2.9−5.1 Pa s, std. dev. 0.7 Pa s) under similar conditions (Figure S1 and Table S1). While considerable sample-to-sample variation was evident, the NT2RepCT specimens showed a weak correlation between concentration and increased viscosity, which became more pronounced above 300 mg mL^{-1} (Figure 1A).

An increase in the dependence of viscosity on concentration can occur in several distinct circumstances. For a polymer solution, this occurs above the overlap concentration, when the

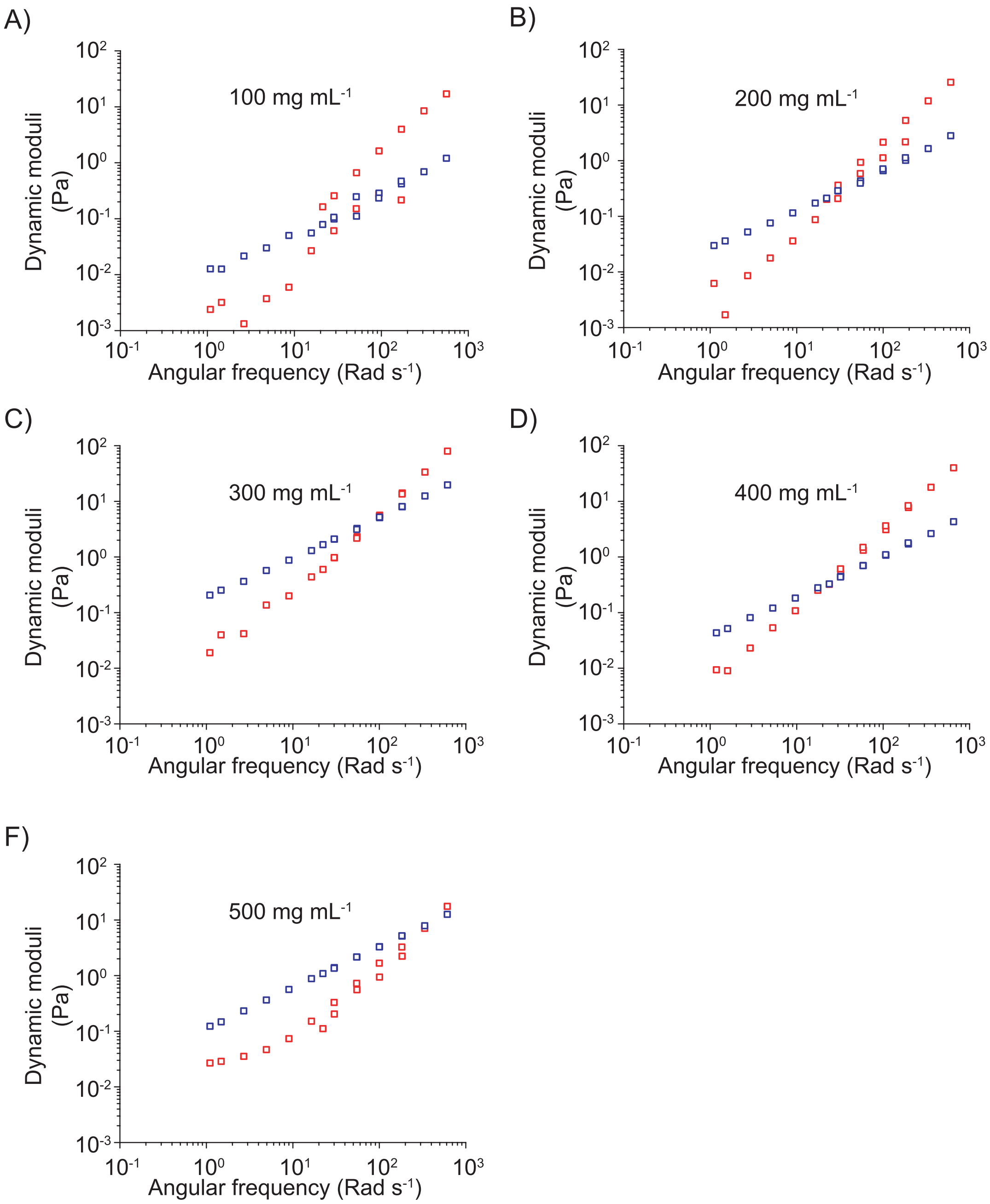

Figure 3. Oscillatory data for different NT2RepCT concentrations at 25 °C. (A) 100, (B) 200, (C) 300, (D) 400, and (E) 500 mg mL^{-1}. Red, G' elastic modulus; blue,G'' viscous modulus.

molecular chains are sufficiently numerous that some overlap is unavoidable. Similar behavior can also be observed in colloidal suspensions, however, when the separation between particles is sufficiently small that the fluid drag on one particle also affects adjacent particles.[31]

Flow history appeared to have a small effect, in that there was a slight tendency for remeasured specimens to exhibit slightly higher viscosities than the initial measurement of the fresh specimen (Figure 1B). The differences appeared more pronounced with the more dilute solutions, suggesting that they may have been due to interactions between the NT2RepCT chains, rather than loss of solvent by evaporation. This may also account for some of the sample variation in the viscosity data presented in Figure 1A.

The shear stress increased with higher flow rates (Figure 1C); however, closer examination revealed that the increase was less than directly proportional to shear rate. Hence, this corresponded to shear-thinning viscosity behavior (Figure 1D).

It was found that the shear rate ramp data could be fitted using the empirical Herschel–Bulkley model,[32−34] combining a yield stress and power-law flow behavior:

$$\sigma(\dot{\gamma}) = \sigma_0 + k(\dot{\gamma})^m \tag{1a}$$

$$\eta(\dot{\gamma}) = \sigma(\dot{\gamma})/\dot{\gamma} \tag{1b}$$

$$=\sigma_0/\dot{\gamma} + k(\dot{\gamma})^{m-1} \tag{1c}$$

https://dx.doi.org/10.1021/acsbiomaterials.0c01308
ACS Biomater. Sci. Eng. 2021, 7, 462−471

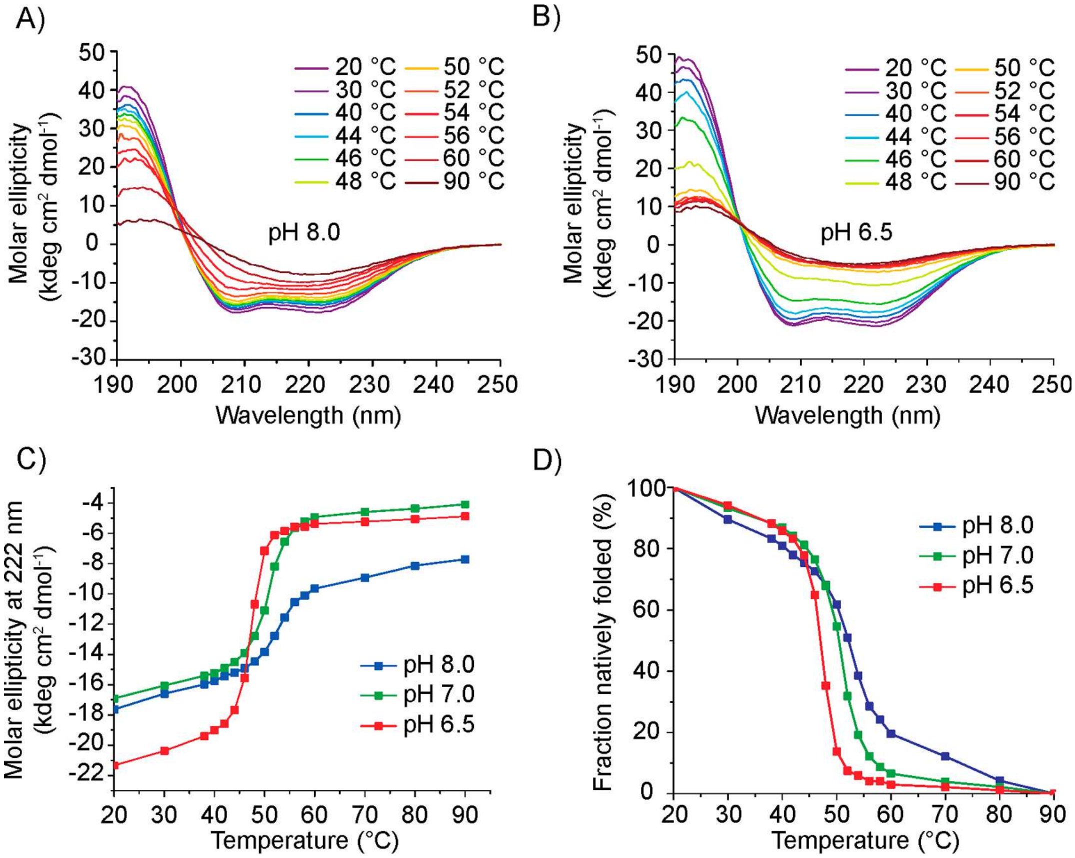

Figure 4. CD spectroscopy of NT2RepCT at 20−90 °C and FTIR spectrum. (A) Spectra of NT2RepCT at pH 8 and (B) pH 6.5 at 20 °C (dark blue) to 90 °C (dark red) show conversion from a predominantly α-helical protein to a β-sheet rich protein. Color coding are the same in A and B. (C) Thermal unfolding of NT2RepCT at pH 8 (blue), 7 (orange) and 6.5 (green) followed by ellipticity at 222 nm. (D) Molar ellipticity at 222 nm converted to fraction natively folded.

According to this model, flow does not start until the shear stress exceeds a threshold value (i.e., the yield stress, σ_0). Then, faster flows are accompanied by further increases in shear stress, as described by the "consistency index" (k) and power law coefficient (m) in eq 1a. The corresponding shear viscosity (i.e., the total shear stress divided by the shear rate, eq 1b), is given by eq 1c. It may be noted that for pure "power law" flow behavior (i.e., $\sigma_0 = 0$), k is equal to the shear viscosity at $\dot{\gamma} = 1$ s^{-1}, whereas values of $m < 1$ correspond to the shear stress increasing subproportionally with shear rate (i.e., shear-thinning). For nonzero σ_0, however, shear-thinning may also arise from the first term in eq 1c.

For the data shown in Figure 1C, D, the yield stress (0.006 Pa s) produced the small upturn in stress or (more obviously) viscosity at low shear rates. Similar flow behavior was also observed for lower concentrations, and further rheological data for a wider range of NT2RepCT solutions are presented in Figure S2.

The rheological parameters extracted from fitting the Herschel−Bulkley model are presented in Figure 2 and Table S2. Most specimens of NT2RepCT solutions exhibited a small yield stress (up to around 0.2 Pa s, Figure 2A); however, no correlation with concentration could be found, suggesting that sample history may have been a more important parameter. While the presence of a small yield stress did not preclude the specimen from flow measurement, it suggests relatively persistent interactions between NT2RepCT chains, possibly due to attraction between the terminal segments.[8,35,36]

The power law index (with mean 0.91, range 0.70−0.98, Figure 2B) also appeared to be essentially independent of concentration. As noted above, $m < 1$ indicated that the shear stress increased subproportionally with shear rate, consistent with shear-thinning.

The consistency indices increased with concentration (Figure 2C), consistent with higher viscosity of the more concentrated solutions. Plotting the consistency index removes any effect due to yield stress, which may be an artifact of sample history; hence, these results may provide a more reliable indication than the data in Figure 1A, regarding the effect of concentration on flow.

A further rheological characteristic of silk dope is its distinctive linear viscoelastic properties, with elastic-like behavior at high angular frequencies, whereas the viscous part dominates at low angular frequencies.[24] Oscillatory measurements of NT2RepCT solutions (Figure 3) showed similar, though not identical, behavior to native dope. More specifically, although many specimens showed the dominance of the elastic (or storage) modulus over the viscous (or loss) modulus (i.e., $G' > G''$) at higher frequencies and a crossover to $G'' > G'$ at lower frequencies, several details were inconsistent with the behavior usually observed with silk feedstocks.[21] First, the data showed a linear dependence of G'' on angular frequency (ω), which is typical of the "terminal

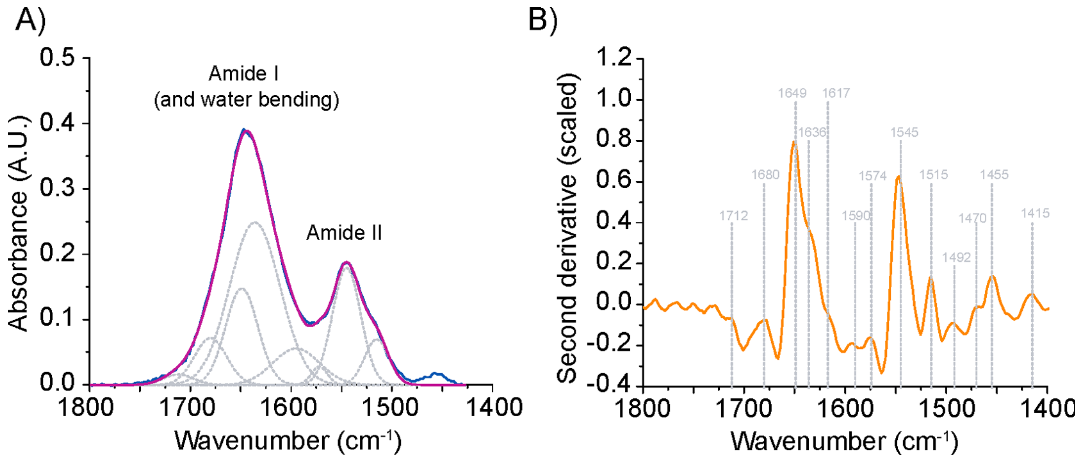

Figure 5. FTIR spectra and second derivative of NT2RepCT. (A) Analysis of amide I and II peaks in the IR spectrum (blue curve) of a NT2RepCT solution (500 mg mL^{-1}, at 37 °C), by curve-fitting a model (magenta) composed of a sum of Gaussian peaks based on the sub-bands (gray, dashed curves) identified in (B) the 2nd derivative spectrum. Note: a linear baseline has been subtracted from the spectrum A and the 2nd derivative has been scaled arbitrarily in the vertical direction, to generate a reasonable numerical scale for the *Y*-axis.

zone". This can be explained by examining the equations for Maxwellian relaxation modes:

$$G''(\omega) = \sum_{n=1}^{n} \frac{g_n \omega \tau_n}{1 + \omega^2 {\tau_n}^2} \tag{2a}$$

$$G'(\omega) = \sum_{n=1}^{n} \frac{g_n \omega^2 {\tau_n}^2}{1 + \omega^2 {\tau_n}^2} \tag{2b}$$

where g_n and τ_n represent the magnitude and relaxation time for the slowest mode. Thus, eq 2a suggests that G'' will become linearly dependent at sufficiently low frequency such that the rheology is dominated by a single "Maxwellian" relaxation mode ($n = 1$) and where $\omega\tau_n < 1$. Because linear behavior of G'' was evident across the entire frequency range investigated (up to 126 rad s^{-1}), this also implies that the slowest relaxation time constant should be smaller than 0.008 s; however, this appears to conflict with observations of a yield stress in shear rate ramp experiments starting at 0.1 s^{-1}. This flow rate should allow sufficient time (more than $10\tau_n$) for any interactions responsible for the stress to relax; assuming exponential relaxation, less than 0.1% of the initial stress should persist.

At the same time, eq 2b suggests that G' should also be dependent on ω^2, whereas lower exponents were found (1.4−1.9). Furthermore, under these conditions, it would be expected that

$$G''(\omega)/G'(\omega) = \frac{1}{\omega\tau_n} \tag{2c}$$

As $\omega\tau_n < 1$ to meet these conditions, it is also expected that $G'' > G'$, and hence, the crossover should not occur in this region. Thus, although the oscillatory data suggested frequency-dependent viscoelasticity for the NT2RepCT solutions, the behavior is not as expected for native silk feedstocks.[21]

pH Effect on NT2RepCT Stability. Next, we investigated the impact of pH on the overall secondary structure content and the stability of NT2RepCT by CD spectroscopy. At pH 8 (as in the storage and production parts of the silk gland), NT2RepCT showed a mainly α-helical structure with two minima at 208 and 222 nm and a positive band at 195 nm at temperatures from 20 to 50 °C (Figure 4) and a gradual loss in α-helical content between 50 and 54 °C (Figure 4A, C). Above 54 °C, a fast transition from mainly α-helical to a β-sheet-dominated conformation took place, as indicated by the appearance of a single broad minimum around 215−220 nm, along with a maximum below 200 nm, followed by a further slightly decreased signal up until 90 °C. As the temperature increased, the CD signal decreased, indicating precipitation of the aggregation-prone protein. In line with this, precipitated protein was visible in the cuvette after the measurements. The heat-induced transition to β-sheets was irreversible upon cooling of the sample (Figure S3A).

To examine the relationship between pH and protein stability, we recorded CD spectra at different temperatures at pH 7.0, 6.5, and 6.0. We found that NT2RepCT at pH 7.0 maintained an α-helix-dominated secondary structure up until 50 °C, compared to 54 °C at pH 8 (Figure S3B). At higher temperatures, the protein underwent conversion to β-sheet conformation. The melting curves confirmed that the transition of the secondary structure occurred at a lower temperature at pH 7.0 compared to pH 8.0 (Figure 4C, D). Lowering the pH to 6.5 or 6.0 caused the protein to precipitate, as evaluated visually and photometrically at 320 nm. However, at pH 6.5, it was still possible to acquire CD spectra of the sample, and these showed a predominantly α-helical structure until 48 °C, whereas above 50 °C, there was a conversion to β-sheet conformation (Figure 4B). Intriguingly, the change in secondary structure was more abrupt at pH 6.5 compared to pH 7.0 and 8.0, where the loss in helical conformation was more gradual (Figure 4A−D and Figure S3B). After the CD temperature ramp measurements at pH 6.5, short fibers were seen in the cuvette (not shown). Upon lowering the pH by only 0.5 units to pH 6.0, the recorded CD spectra showed a very low amplitude due to aggregation that prevented estimation of the secondary structure content (Figure S3C).

The initial conformation of the concentrated NT2RepCT protein was also investigated by analyzing the amide I peak in the IR spectrum (Figure 5A). On the basis of the second derivative spectrum (Figure 5B), four main sub-bands (at 1617, 1636, 1649, and 1680 cm^{-1}) were identified within the amide I region (1600 to 1700 cm^{-1}), whereas sub-bands (at 1590 and 1712 cm^{-1}) made smaller contributions to the peak. Fitting a model based on a sum of Gaussian peaks showed that

https://dx.doi.org/10.1021/acsbiomaterials.0c01308
ACS Biomater. Sci. Eng. 2021, 7, 462−471

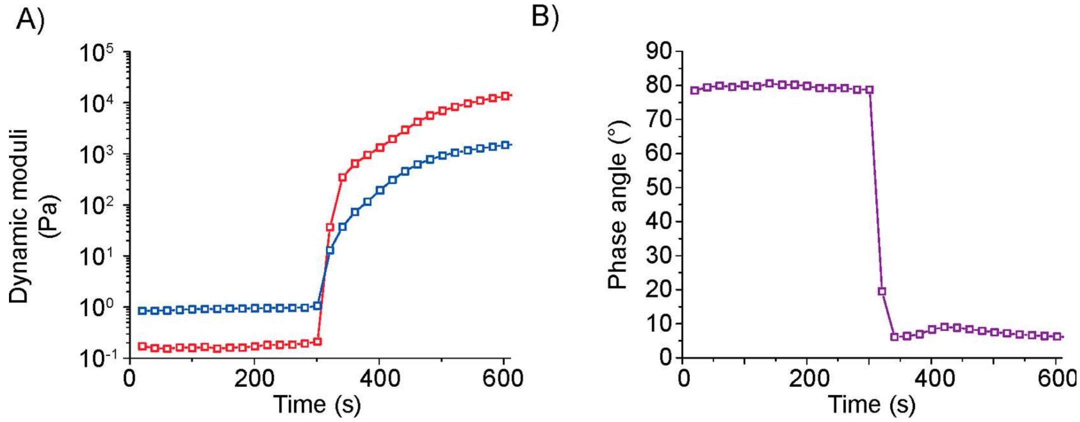

Figure 6. Oscillatory measurements of NT2RepCT during pH-induced phase-transition. (A) Storage modulus G' (red) and loss modulus G'' (blue) during acetic acid vapor (at approximately 300 s) immediately induced phase-transition of 300 mg mL^{-1} NT2RepCT. (B) Changes in phase angle during pH-induced phase transition.

the amide I peak was dominated by the bands centered around 1636, 1649, and 1680 cm^{-1}; Percot et al. previously ascribed these to α-helix and β-turn components in dissolved silk proteins,[37] broadly in agreement with the results from the CD measurements.

Changes in pH can Induce Phase Transition of NT2RepCT. Next, we studied the kinetics of pH induced phase-transition by rheology, a technique that allows measurements at concentrations that are similar to the spidroin concentrations in the gland (whereas CD spectroscopy requires diluted samples). In line with the CD spectroscopy results, a pH-sensitive NT2RepCT phase-transition was observed upon exposure to acetic acid vapor, as indicated by a larger elastic modulus than viscous modulus and a rapid decrease in the phase angle below 45° (Figure 6A, B).

■ DISCUSSION

Success in the quest for making truly biomimetic spider silk fibers requires replication of all the main features of the native spinning process, including the properties of the spinning dope. Solutions of the miniature spidroin NT2RepCT can be concentrated to >500 mg mL^{-1}, and have already been successfully spun into fibers in a biomimetic process that recapitulates important molecular mechanisms of native silk formation.[29] However, whether the NT2RepCT dope captures the main features of native silk dope, i.e., high viscosity at low shear rates, shear-thinning, and viscoelasticity,[24] is not known.

Initially, we studied the viscosity and shear-thinning of NT2RepCT dope and could show that NT2RepCT dope indeed displayed a shear-thinning behavior (Figure 1C, D). This property could explain why extrusion of the highly concentrated dope through a thin glass capillary in a spinning device could be achieved using only low-pressure pumps.[29] During shear-thinning, loss of molecular entanglement and disruption of other frequency-dependent intermolecular interactions enables the proteins to move more easily, thus decreasing the viscosity of the solution.[38] It should be noted though, that compared to native dope, the decrease in viscosity was smaller (3-fold vs 35-fold) and the initial viscosity of the NT2RepCT dope was much lower compared to the native feedstock (Figure 1D).[24] One possible explanation for the lower viscosity observed may be that the small size of NT2RepCT compared to full-length spidroins (66 kDa vs 600 kDa, as constitutive dimers) correlates with fewer intermolecular interactions.[39,40] Another potential explanation may involve the "sticky reptation" mechanism that was recently identified in *Bombyx mori* silk feedstock, by which the viscosity is controlled by the relative concentrations of mono- and divalent cations.[41−43]

Native silk dope probably organizes into micelles where the terminal domains form the shell and the repetitive regions are shielded in the center.[44] NT2RepCT in solution also forms assemblies of 4−6 molecules, which are around 7−11 nm in diameter.[29,30] In this study, we observed that the shear viscosity at 1 s^{-1} of NT2RepCT (Figure 1A), or the consistency index from fitting the Herschel−Bulkley model (Figure 2C) correlated with the concentration. This suggests that the NT2RepCT micelles interact, and in line with this, increased concentration of NT2RepCT leads to increased viscosity of the dope. This is interesting because fibers spun from reconstituted silk dope with high viscosity have been reported to show improved mechanical properties.[45] Consequently, one possible way of increasing the mechanical properties of NT2RepCT fibers may be to increase the viscosity, e.g., by increasing the molecular weight of the protein—ideally by increasing the number of repetitive segments.

Viscoelastic behavior, where the viscous part is dominating at low frequencies and elastic properties at higher frequencies under oscillatory measurements,[20] is another important feature of native silk dope that is recapitulated by NT2RepCT (Figure 3). However, the values of the moduli and the shape of the graphs differ between NT2RepCT and native dopes, although the degree of variability is comparable.[21,24]

The spinning process is accompanied by significant structural changes of the spidroins, which are initiated by decreased pH and increased shear forces in the duct.[8,9,20] A typical spidroin contains three distinct parts: nonrepetitive NT and CT that flank an extensive repetitive region.[39,46−49] The repetitive part is generally composed of up to 100 alternating repeats of poly alanine and glycine-rich regions, which form mainly random coil and helical secondary structures in the dope.[7,50−52] The terminal domains are α-helical and function as regulators of fiber formation, acting through conformational changes. As pH is lowered, the NT dimerizes but keeps its overall secondary structure content while the CT unfolds and goes into β-sheet conformation.[8,46,48,53−56] By using CD spectroscopy, we found that NT2RepCT is mainly in an α-

https://dx.doi.org/10.1021/acsbiomaterials.0c01308
ACS Biomater. Sci. Eng. 2021, 7, 462−471

helical conformation at pH 8.0, 7.0, and 6.5 (Figure 4A, B and Figure S3B), which is expected from the α-helical terminal domains and predicted α-helical conformation of the poly alanine regions, and also in line with previous findings where NT2RepCT was studied by NMR spectroscopy.[30] The extreme solubility of NT2RepCT enabled us to study this protein in solution by FTIR spectroscopy, which confirmed that, even at high concentrations, the protein conformation was dominated by α-helical and β-turn components (Figure 5). Previous FTIR spectroscopy studies on gland content also suggested the presence of α-helices accompanied by unidentified secondary structures.[6] Furthermore, studies of the melting temperature of NT2RepCT by CD spectroscopy at physiologically relevant pHs show that as pH is lowered, the stability of NT2RepCT decreases (Figure 4C). We speculate that this is mainly due to a pH-dependent destabilization of CT, which has previously been shown for this domain in isolation.[8,46]

■ CONCLUSION

In this study, we show that NT2RepCT dope recapitulates many features of the native silk dope, including shear-thinning, crossover of the viscoelastic moduli at increased frequencies, and structural changes in response to changes in pH. We propose that the presence of native-like characteristics in recombinant spidroin dopes is key to establishing biomimetic spinning procedures.

■ ASSOCIATED CONTENT

Supporting Information

The Supporting Information is available free of charge at https://pubs.acs.org/doi/10.1021/acsbiomaterials.0c01308.

> Viscosity measurements of aqueous poly(N-isopropylacrylamide) solutions to compare this synthetic polymer with the material characterized here; shear rate ramp and viscosity of 100, 200, 300, and 400 mg mL^{-1} NT2RepCT; CD spectra showing irreversibility of thermal denaturation, temperature unfolding at pH 7 and pH 6 (PDF)

■ AUTHOR INFORMATION

Corresponding Authors

Chris Holland − *Department of Materials Science and Engineering, The University of Sheffield, Sheffield S1 3JD, United Kingdom;* orcid.org/0000-0003-0913-2221; Email: christopher.holland@sheffield.ac.uk

Anna Rising − *Department of Neurobiology, Care Sciences and Society (NVS), Karolinska Institutet, Huddinge 141 52, Sweden; Department of Anatomy, Physiology and Biochemistry, Swedish University of Agricultural Sciences, Uppsala 750 07, Sweden;* orcid.org/0000-0002-1872-1207; Email: anna.rising@ki.se

Authors

Tina Arndt − *Department of Neurobiology, Care Sciences and Society (NVS), Karolinska Institutet, Huddinge 141 52, Sweden*

Peter R. Laity − *Department of Materials Science and Engineering, The University of Sheffield, Sheffield S1 3JD, United Kingdom*

Jan Johansson − *Department of Neurobiology, Care Sciences and Society (NVS), Karolinska Institutet, Huddinge 141 52, Sweden;* orcid.org/0000-0002-8719-4703

Complete contact information is available at: https://pubs.acs.org/10.1021/acsbiomaterials.0c01308

Author Contributions

The manuscript was written through contributions of all authors. All authors have given approval to the final version of the manuscript.

Funding

This project has received funding from the European Research Council (ERC) under the European Union's Horizon 2020 research and innovation program (grant agreement 815357), the Center for Innovative Medicine (CIMED) at Karolinska Institutet, and Stockholm City Council, SFO Regen FOR 4−1364/2019, the Swedish Research Council (2019−01257), and Formas (2019−00427). P.R.L. and C.H. are grateful to the European Union's Horizon 2020 research and innovation program under grant agreement 713475 for funding this work.

Notes

The authors declare no competing financial interest.

■ ABBREVIATIONS

CD, circular dichroism; FTIR, Fourier transform infrared spectroscopy; IMAC, immobilized metal affinity chromatography; IPTG, Isopropyl β-d-1-thiogalactopyranoside; MaSp1, major ampullate spidroin 1; NT2RepCT, chimeric minispidroin composed of NT from *Euprosthenops australis*; MaSp1, a repetitive part consisting of two poly alanine and two glycine-rich repeat regions from *E. australis* MaSp1 and a CT from *Araneus ventricosus* minor ampullate spidroin

■ REFERENCES

(1) Salehi, S.; Koeck, K.; Scheibel, T. *Molecules* **2020**, *25*, 737.

(2) Omenetto, F. G.; Kaplan, D. L. New opportunities for an ancient material. *Science* **2010**, *329* (5991), 528−31.

(3) Koeppel, A.; Holland, C. Progress and Trends in Artificial Silk Spinning: A Systematic Review. *ACS Biomater. Sci. Eng.* **2017**, *3* (3), 226−237.

(4) Rising, A.; Johansson, J. Toward spinning artificial spider silk. *Nat. Chem. Biol.* **2015**, *11* (5), 309−15.

(5) Xu, M.; Lewis, R. V. Structure of a protein superfiber: spider dragline silk. *Proc. Natl. Acad. Sci. U. S. A.* **1990**, *87* (18), 7120−4.

(6) Hijirida, D. H.; Do, K. G.; Michal, C.; Wong, S.; Zax, D.; Jelinski, L. W. 13C NMR of Nephila clavipes major ampullate silk gland. *Biophys. J.* **1996**, *71* (6), 3442−7.

(7) van Beek, J. D.; Hess, S.; Vollrath, F.; Meier, B. H. The molecular structure of spider dragline silk- Folding and orientation of the protein backbone. *Proc. Natl. Acad. Sci. U. S. A.* **2002**, *99* (16), 10266−71.

(8) Andersson, M.; Chen, G.; Otikovs, M.; Landreh, M.; Nordling, K.; Kronqvist, N.; Westermark, P.; Jornvall, H.; Knight, S.; Ridderstrale, Y.; Holm, L.; Meng, Q.; Jaudzems, K.; Chesler, M.; Johansson, J.; Rising, A. Carbonic anhydrase generates CO2 and H+ that drive spider silk formation via opposite effects on the terminal domains. *PLoS Biol.* **2014**, *12* (8), e1001921.

(9) Rousseau, M. E.; Lefevre, T.; Beaulieu, L.; Asakura, T.; Pezolet, M. Study of protein conformation and orientation in silkworm and spider silk fibers using Raman microspectroscopy. *Biomacromolecules* **2004**, *5* (6), 2247−2257.

(10) Knight, D.; Vollrath, F. Changes in element composition along the spinning duct in a Nephila spider. *Naturwissenschaften* **2001**, *88* (4), 179−182.

(11) Sparkes, J.; Holland, C. Analysis of the pressure requirements for silk spinning reveals a pultrusion dominated process. *Nat. Commun.* **2017**, *8* (1), 594.
(12) Sparkes, J.; Holland, C. The Energy Requirements for Flow-Induced Solidification of Silk. *Macromol. Biosci.* **2019**, *19* (3), e1800229.
(13) Simmons, A.; Ray, E.; Jelinski, L. W. Solid-State 13C NMR of Nephila clavipes Dragline Silk Establishes Structure and Identity of Crystalline Regions. *Macromolecules* **1994**, *27* (18), 5235−5237.
(14) Kümmerlen, J.; van Beek, J. D.; Vollrath, F.; Meier, B. H. Local Structure in Spider Dragline Silk Investigated by Two-Dimensional Spin-Diffusion Nuclear Magnetic Resonance†. *Macromolecules* **1996**, *29* (8), 2920−2928.
(15) Simmons, A. H.; Michal, C. A.; Jelinski, L. W. Molecular orientation and two-component nature of the crystalline fraction of spider dragline silk. *Science* **1996**, *271* (5245), 84−87.
(16) Asakura, T. Structure and Dynamics of Spider Silk Studied with Solid-State Nuclear Magnetic Resonance and Molecular Dynamics Simulation. *Molecules* **2020**, *25* (11), 2634.
(17) McGill, M.; Holland, G. P.; Kaplan, D. L. Experimental Methods for Characterizing the Secondary Structure and Thermal Properties of Silk Proteins. *Macromol. Rapid Commun.* **2019**, *40* (1), e1800390.
(18) Xu, D.; Yarger, J. L.; Holland, G. P. Exploring the backbone dynamics of native spider silk proteins in Black Widow silk glands with solution-state NMR spectroscopy. *Polymer* **2014**, *55* (16), 3879−3885.
(19) Matsumoto, A.; Lindsay, A.; Abedian, B.; Kaplan, D. L. Silk fibroin solution properties related to assembly and structure. *Macromol. Biosci.* **2008**, *8* (11), 1006−18.
(20) Vollrath, F.; Knight, D. P. Liquid crystalline spinning of spider silk, Review. *Nature* **2001**, *410* (6828), 541−8.
(21) Laity, P. R.; Gilks, S. E.; Holland, C. Rheological behaviour of native silk feedstocks. *Polymer* **2015**, *67*, 28−39.
(22) Bell, A. L.; Peakall, D. B. Changes in Fine Structure during Silk Protein Production in the Ampullate Gland of the Spider Araneus Sericatus. *J. Cell Biol.* **1969**, *42* (1), 284−295.
(23) Kojic, N.; Bico, J.; Clasen, C.; McKinley, G. H. Ex vivo rheology of spider silk. *J. Exp. Biol.* **2006**, *209* (21), 4355−4362.
(24) Holland, C.; Terry, A. E.; Porter, D.; Vollrath, F. Comparing the rheology of native spider and silkworm spinning dope. *Nat. Mater.* **2006**, *5* (11), 870−4.
(25) Holland, C.; Vollrath, F.; Ryan, A. J.; Mykhaylyk, O. O. Silk and synthetic polymers: reconciling 100 degrees of separation. *Adv. Mater.* **2012**, *24* (1), 105−109.
(26) Holland, C.; Terry, A. E.; Porter, D.; Vollrath, F. Natural and unnatural silks. *Polymer* **2007**, *48* (12), 3388−3392.
(27) Boulet-Audet, M.; Holland, C.; Gheysens, T.; Vollrath, F. Dry-Spun Silk Produces Native-Like Fibroin Solutions. *Biomacromolecules* **2016**, *17* (10), 3198−3204.
(28) Rammensee, S.; Slotta, U.; Scheibel, T.; Bausch, A. R. Assembly mechanism of recombinant spider silk proteins. *Proc. Natl. Acad. Sci. U. S. A.* **2008**, *105* (18), 6590−5.
(29) Andersson, M.; Jia, Q.; Abella, A.; Lee, X. Y.; Landreh, M.; Purhonen, P.; Hebert, H.; Tenje, M.; Robinson, C. V.; Meng, Q.; Plaza, G. R.; Johansson, J.; Rising, A. Biomimetic spinning of artificial spider silk from a chimeric minispidroin. *Nat. Chem. Biol.* **2017**, *13* (3), 262−264.
(30) Otikovs, M.; Andersson, M.; Jia, Q.; Nordling, K.; Meng, Q.; Andreas, L. B.; Pintacuda, G.; Johansson, J.; Rising, A.; Jaudzems, K. Degree of Biomimicry of Artificial Spider Silk Spinning Assessed by NMR Spectroscopy. *Angew. Chem., Int. Ed.* **2017**, *56* (41), 12571−12575.
(31) Larson, R. G. *The Structure and Rheology of Complex Fluids*; Oxford University Press: 1999.
(32) Herschel, W. H.; Bulkley, R. Konsistenzmessungen von Gummi-Benzollösungen. *Colloid Polym. Sci.* **1926**, *39* (4), 291−300.
(33) Papanastasiou, T. C.; Boudouvis, A. G. Flows of viscoplastic materials: Models and computations. *Comput. Struct.* **1997**, *64* (1−4), 677−694.
(34) Mueller, S.; Llewellin, E. W.; Mader, H. M. The rheology of suspensions of solid particles. *Proc. R. Soc. London, Ser. A* **2010**, *466* (2116), 1201−1228.
(35) Bauer, J.; Scheibel, T. Dimerization of the Conserved N-Terminal Domain of a Spider Silk Protein Controls the Self-Assembly of the Repetitive Core Domain. *Biomacromolecules* **2017**, *18* (8), 2521−2528.
(36) Gauthier, M.; Leclerc, J.; Lefevre, T.; Gagne, S. M.; Auger, M. Effect of pH on the structure of the recombinant C-terminal domain of Nephila clavipes dragline silk protein. *Biomacromolecules* **2014**, *15* (12), 4447−54.
(37) Percot, A.; Colomban, P.; Paris, C.; Dinh, H. M.; Wojcieszak, M.; Mauchamp, B. Water dependent structural changes of silk from Bombyx mori gland to fibre as evidenced by Raman and IR spectroscopies. *Vib. Spectrosc.* **2014**, *73*, 79−89.
(38) Yasuda, K.; Armstrong, R. C.; Cohen, R. E. Shear flow properties of concentrated solutions of linear and star branched polystyrenes. *Rheol. Acta* **1981**, *20* (2), 163−178.
(39) Ayoub, N. A.; Garb, J. E.; Tinghitella, R. M.; Collin, M. A.; Hayashi, C. Y. Blueprint for a high-performance biomaterial: full-length spider dragline silk genes. *PLoS One* **2007**, *2* (6), e514.
(40) Babb, P. L.; Lahens, N. F.; Correa-Garhwal, S. M.; Nicholson, D. N.; Kim, E. J.; Hogenesch, J. B.; Kuntner, M.; Higgins, L.; Hayashi, C. Y.; Agnarsson, I.; Voight, B. F. The Nephila clavipes genome highlights the diversity of spider silk genes and their complex expression. *Nat. Genet.* **2017**, *49* (6), 895−903.
(41) Laity, P. R.; Baldwin, E.; Holland, C. Changes in Silk Feedstock Rheology during Cocoon Construction: The Role of Calcium and Potassium Ions. *Macromol. Biosci.* **2019**, *19* (3), e1800188.
(42) Schaefer, C.; Laity, P. R.; Holland, C.; McLeish, T. C. B. Silk Protein Solution: A Natural Example of Sticky Reptation. *Macromolecules* **2020**, *53* (7), 2669−2676.
(43) Koeppel, A.; Laity, P. R.; Holland, C. The influence of metal ions on native silk rheology. *Acta Biomater.* **2020**, *117*, 204−212.
(44) Jin, H. J.; Kaplan, D. L. Mechanism of silk processing in insects and spiders. *Nature* **2003**, *424* (6952), 1057−1061.
(45) Park, B. K.; Um, I. C. Effect of molecular weight on electro-spinning performance of regenerated silk. *Int. J. Biol. Macromol.* **2018**, *106*, 1166−1172.
(46) Hagn, F.; Eisoldt, L.; Hardy, J. G.; Vendrely, C.; Coles, M.; Scheibel, T.; Kessler, H. A conserved spider silk domain acts as a molecular switch that controls fibre assembly. *Nature* **2010**, *465* (7295), 239−42.
(47) Rising, A.; Hjälm, G.; Engström, W.; Johansson, J. N-Terminal Nonrepetitive Domain Common to Dragline, Flagelliform, and Cylindriform Spider Silk Proteins. *Biomacromolecules* **2006**, *7* (11), 3120−4.
(48) Askarieh, G.; Hedhammar, M.; Nordling, K.; Saenz, A.; Casals, C.; Rising, A.; Johansson, J.; Knight, S. D. Self-assembly of spider silk proteins is controlled by a pH-sensitive relay. *Nature* **2010**, *465* (7295), 236−8.
(49) Ittah, S.; Cohen, S.; Garty, S.; Cohn, D.; Gat, U. An Essential Role for the C-Terminal Domain of A Dragline Spider Silk Protein in Directing Fiber Formation. *Biomacromolecules* **2006**, *7* (6), 1790−1795.
(50) Jenkins, J. E.; Sampath, S.; Butler, E.; Kim, J.; Henning, R. W.; Holland, G. P.; Yarger, J. L. Characterizing the secondary protein structure of black widow dragline silk using solid-state NMR and X-ray diffraction. *Biomacromolecules* **2013**, *14* (10), 3472−83.
(51) Xu, D.; Shi, X.; Thompson, F.; Weber, W. S.; Mou, Q.; Yarger, J. L. Protein secondary structure of Green Lynx spider dragline silk investigated by solid-state NMR and X-ray diffraction. *Int. J. Biol. Macromol.* **2015**, *81*, 171−9.
(52) Holland, G. P.; Jenkins, J. E.; Creager, M. S.; Lewis, R. V.; Yarger, J. L. Solid-State NMR Investigation of Major and Minor

Ampullate Spider Silk in the Native and Hydrated States. *Biomacromolecules* **2008**, *9*, 651.

(53) Kronqvist, N.; Otikovs, M.; Chmyrov, V.; Chen, G.; Andersson, M.; Nordling, K.; Landreh, M.; Sarr, M.; Jornvall, H.; Wennmalm, S.; Widengren, J.; Meng, Q.; Rising, A.; Otzen, D.; Knight, S. D.; Jaudzems, K.; Johansson, J. Sequential pH-driven dimerization and stabilization of the N-terminal domain enables rapid spider silk formation. *Nat. Commun.* **2014**, *5*, 3254.

(54) Hedhammar, M.; Rising, A.; Grip, S.; Martinez, A. S.; Nordling, K.; Casals, C.; Stark, M.; Johansson, J. Structural properties of recombinant nonrepetitive and repetitive parts of major ampullate spidroin 1 from Euprosthenops australis: implications for fiber formation. *Biochemistry* **2008**, *47* (11), 3407−17.

(55) Landreh, M.; Askarieh, G.; Nordling, K.; Hedhammar, M.; Rising, A.; Casals, C.; Astorga-Wells, J.; Alvelius, G.; Knight, S. D.; Johansson, J.; Jornvall, H.; Bergman, T. A pH-dependent dimer lock in spider silk protein. *J. Mol. Biol.* **2010**, *404* (2), 328−36.

(56) Jaudzems, K.; Askarieh, G.; Landreh, M.; Nordling, K.; Hedhammar, M.; Jornvall, H.; Rising, A.; Knight, S. D.; Johansson, J. pH-dependent dimerization of spider silk N-terminal domain requires relocation of a wedged tryptophan side chain. *J. Mol. Biol.* **2012**, *422* (4), 477−87.

https://dx.doi.org/10.1021/acsbiomaterials.0c01308
ACS Biomater. Sci. Eng. 2021, 7, 462−471